Electronic Supplementary Information for:

Development of Angle-adjustable Photonic Crystal Fluorescence Platform for Sensitive Detection of Oxytetracycline

Yunhuan Huang [a,1], *Jiaheng Zhang* [a,b,1], *Bo Sui* [a], *Guobi Chai* [a], *Ajuan Yu* [a], *Sheng Chen* [a], *Miaomiao Zhang* [a], *Shusheng Zhang* [b], *Yanhao Zhang* [c,*], *Wuduo Zhao* [a,c,*]

[a] College of Chemistry, Zhengzhou University, Zhengzhou 450001, P. R China

[b] Food Laboratory of Zhongyuan · Zhengzhou University, Luohe 462300, P. R China

[c] College of Ecology and Environment, Zhengzhou University, Zhengzhou 450001, P. R China

[1] These authors contributed equally

* Corresponding authors

1. Experimental sections

1.1. Reagents and materials

Gold (III) chloride trihydrate ($HAuCl_4 \cdot 3H_2O$), bovine serum albumin (BSA), styrene, sodium hydroxide (NaOH), polyvinylpyrrolidone (PVP) potassium persulfate (KPS), sodium dodecyl sulfate (SDS), oxytetracycline (OTC), amoxicillin (AMX), ampicillin (AMP), amikacin sulfate (AMK), gentamicin (GEN), cephalexin monohydrate (LEX), clindamycin hydrochloride (CLI), sulfonamide (SM), oxacillin sodium (OXCL), ciprofloxacin (CRO), cefaclor (CFR), ceftriaxone sodium (CXM), ofloxacin (OFX) was acquired from Macklin. All the reagents were used as received without further purification. Ultra-pure Milli Q water (18.2 MΩ.cm, Merck) was utilized throughout the experiment.

1.2. Characterizations

Transmission electron microscope (TEM) images were acquired using a Thermo Fisher Scientific/Talos L120CG2 system. The periodic arrangement scanning electron microscopy (SEM) images were examined with a Zeiss/Auriga-bu system. X-ray photoelectron spectroscopy (XPS) data were obtained using the AXIS Supra instrument. Fourier transform infrared (FT-IR) spectroscopies were performed using the Tracer-100 Infrared spectrometer. The visual colors of CPCs were validated using the CIE (International Commission on Illumination) color space chromaticity diagram.

1.3. Preparation of monodispersed PS microspheres and fabrication of PS-based CPCs

The monodisperse polystyrene (PS) microspheres were synthesized through an emulsion polymerization method.[1] The PS-based colloidal photonic crystals (CPCs) were fabricated using a vertical deposition method. Initially, the dried polystyrene microspheres were dispersed uniformly in an ethanol solution through ultrasonication for 2 hours. Subsequently, different CPCs with varying photonic band gaps were prepared by vertically depositing 10 mL PS dispersion solutions onto quartz glass slides. The deposition process was conducted at a constant temperature of 35°C. Following the evaporation of ethanol, the close-packed periodic arrangement of polystyrene microspheres exhibited vibrant colors, signifying the formation of CPCs.

1.4. Synthesis of fluorescent BSA-AuNCs and fabrication of BSA-AuNCs-CPCs

A one-pot green synthesis method was employed to obtain bovine serum albumin (BSA) capped fluorescent gold nanoclusters (AuNCs) following a previously reported procedure.[2] To fabricate the fluorescent sensor, BSA-AuNCs were dripped onto the surface of the colloidal photonic crystals (CPCs) followed by drying at room temperature. Subsequently, a fixed volume of OTC in acetone solution at various molar concentrations was added to the sensor and dried at room temperature. Control samples were prepared by adding an equal amount of BSA-AuNCs drops onto a glass substrate and allowing them to dry.

2. Results and Discussion

2.1 The characterization of BSA-capped fluorescent gold nanoclusters (BSA-AuNCs)

Gold nanoclusters display fluorescence upon excitation by specific wavelengths. Characterized by their simple preparation methods and unique physicochemical properties, these nanoclusters outperform traditional fluorescent materials. Bovine serum albumin (BSA) is commonly favored as a template for synthesizing nanoclusters owing to its abundant protein content, which is vital for applications in fluorescence-based quantitative analysis.[3] Consequently, BSA-AuNCs have been widely employed in the detection of various targets, serving as the model material in this study. To confirm the successful synthesis of BSA-AuNCs, we employed an array of characterization techniques, including FT-IR spectroscopy, XPS, UV-vis spectroscopy, and TEM. The FT-IR spectra for both native BSA and BSA-capped AuNCs revealed two distinct absorption bands at 1655 cm^{-1} and 1526 cm^{-1}. These bands corresponded to the amide I band, primarily associated with C=O

stretching vibrations, and the amide II band, arising from N-H bending vibrations, respectively, thereby indicating the preservation of BSA's secondary structure in the BSA-AuNCs (Figure S1A). Furthermore, absorption bands observed at 2963 cm^{-1} and 3302 cm^{-1} were attributed to the C-H and N-H/O-H characteristic vibrations of BSA, respectively, highlighting the retention of BSA's structural integrity within the BSA-AuNCs. Subtle variances observed in the FT-IR spectra between native BSA and BSA-AuNCs affirmed the stability and maintenance of BSA's conformation post-nanocluster formation. In the XPS spectra, binding energies of Au $4f_{5/2}$ (84.5 eV) and $4f_{7/2}$ (80.8 eV) were indicative of the predominance of gold atoms (Figure S1B). A peak at 159.7 eV, assignable to S $2p_{3/2}$, elucidated the interaction between gold atoms and BSA's thiol groups, thus confirming the successful encapsulation of AuNCs by BSA (Figure S1C). TEM image revealed that the BSA-AuNCs are predominantly spherical with a uniform size distribution, with an average diameter of approximately 2 nm (Figure S1E). The fluorescence spectra of these BSA-AuNCs (Figure S1D), exhibited an emission wavelength at 675 nm upon excitation at 513 nm, yielding a significant Stokes shift of 162 nm. This considerable shift effectively minimizes interference between excitation and emission signals, underscoring the suitability of BSA-AuNCs for fluorescence-based applications. Additionally, under ambient daylight, BSA-AuNCs displayed a brown color but emit intense red fluorescence when exposed to ultraviolet light at 365 nm. The fluorescence stability of the BSA-AuNCs, demonstrated that the initial fluorescence intensity is maintained at over 80% even after 60 minutes of continuous, intense excitation (Figure S1F). This durability indicated the robustness of the fluorescence emission under prolonged excitation, highlighting the promising utility of BSA-AuNCs in applications necessitating stable fluorescent markers.

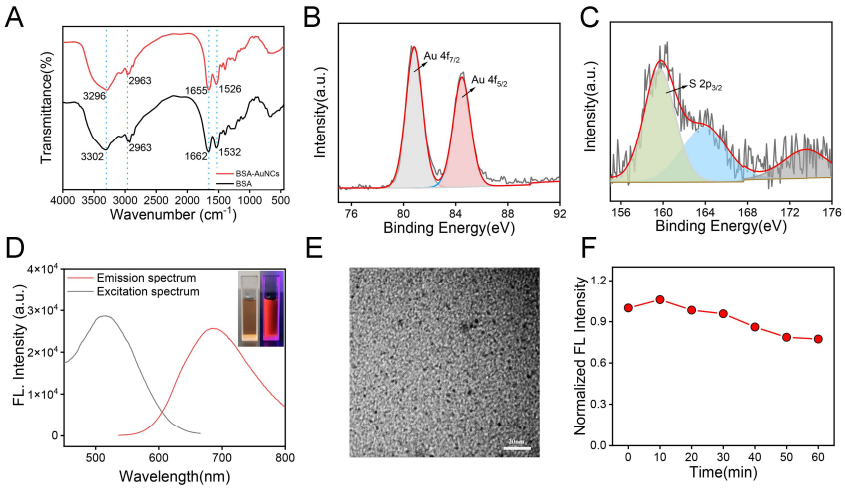

Figure S1 (A) FT-IR spectra of BSA and BSA-AuNCs, (B, C) XPS high-resolution spectra of Au 4f, S 2p, (D) fluorescence excitation and emission spectra of BSA-AuNCs, Inset: Digital photographs of BSA-AuNCs under visible light and UV light (365 nm), (E) TEM image of the synthesized BSA-AuNCs, (F) photostability of the BSA-AuNCs within 60 min.

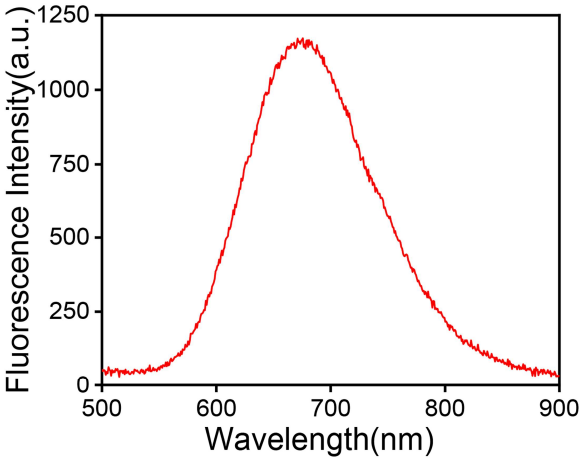

Figure S2. Fluorescence spectra of BSA-AuNCs-CPC.

2.2 The optimization of detection system conditions

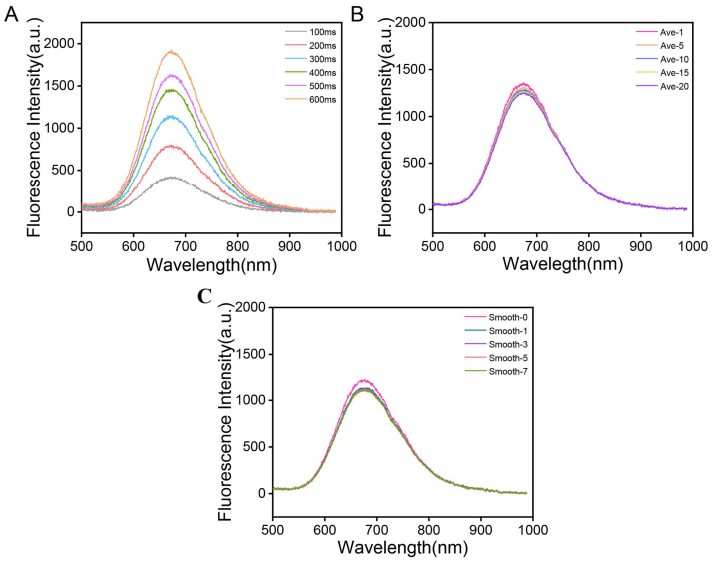

Figure S3. (A) Fluorescence spectra of different integration time; (B) Fluorescence spectra of different average frequency; (C) Fluorescence spectra of different smoothing frequency.

2.3 The characterization of CPCs

PS microspheres of varying diameters were synthesized via emulsion polymerization, subsequently self-assembling into colloidal photonic crystals (CPCs). Scanning electron microscope (SEM) images of CPCs, as presented in Figures S4A and S5, illustrated the assembly of these microspheres into CPCs, characterized by a smooth surface and an approximate diameter of 280 nm. These CPCs exhibited a highly ordered face-centered cubic (fcc) structure, with their (111) plane oriented parallel to the substrate surface. Further SEM analysis, detailed in Figure S1, displayed CPCs with diameters of 230 nm, 250 nm, 300 nm, and 320 nm (denoted as CPC_{230}, CPC_{250}, CPC_{300}, and CPC_{320}, respectively), underscoring the versatility in controlling CPC dimensions. The CIE color coordinates for CPC_{280} indicated a distinct and easily discernible coloration. A comprehensive set of CIE color coordinates for these self-assembled CPCs, detailed in Figure S6, showcased the tunability of optical properties across the spectrum of CPC structures. Reflectance spectroscopy of CPC_{280} revealed a peak reflectance wavelength at 673 nm, attributed to the periodic arrangement of PS particles, aligning with the Bragg scattering effect. The relationship between the maximum reflectance wavelength of CPCs (λ), the diameter of the PS

nanoparticles (D), and the angle (θ) between the incident light and the surface of the CPCs' can be described by Equation (1).

$$\lambda = 2\sqrt{\frac{2}{3}}D\sqrt{n_{eff}^2 - sin^2\theta} \quad (1)$$

Furthermore, the average effective refraction coefficient of the CPCs, n_{eff} can be determined by Equation (2):

$$n_{eff}^2 = fn_{sphe}^2 + (1-f)n_{air}^2 \quad (2)$$

In Equation (2), f represents the filling fraction of PS in the CPCs (0.74), while n_{sphe} and n_{air} denote the refractive indices of PS microspheres and air, respectively.

Reflectance spectra of four different types of CPCs assembled using monodisperse PS microspheres with diameters of 230 nm, 250 nm, 300 nm, and 320 nm are presented in Figure S7. The observed bandgap positions at 559 nm, 607 nm, 711 nm, and 756 nm are basically consistent with those predicted by the Bragg scattering equation at 552 nm, 600 nm, 720 nm and 767 nm, indicating the successful preparation and the high quality of fabricated PS photonic crystals.

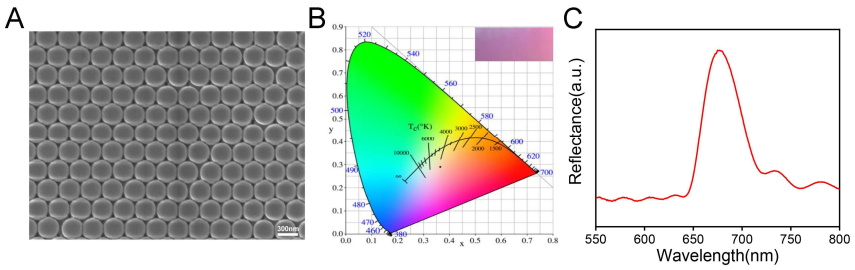

Figure S4 (A) SEM micrograph of colloidal photonic crystal CPC_{280}, (B) CIE (International Commission on Illumination) chromaticity diagram showing the (x, y) color coordinates of CPC_{280}, inset: Digital photograph of CPC_{280}, (C) Reflectance spectra of fabricated colloidal photonic crystal CPC_{280}.

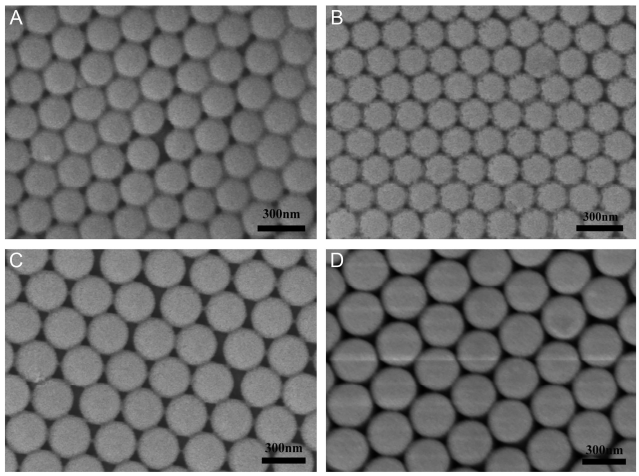

Figure S5. SEM micrograph of colloidal photonic crystal: (A) CPC_{230}, (B) CPC_{250}, (C) CPC_{300}, (D) CPC_{320}.

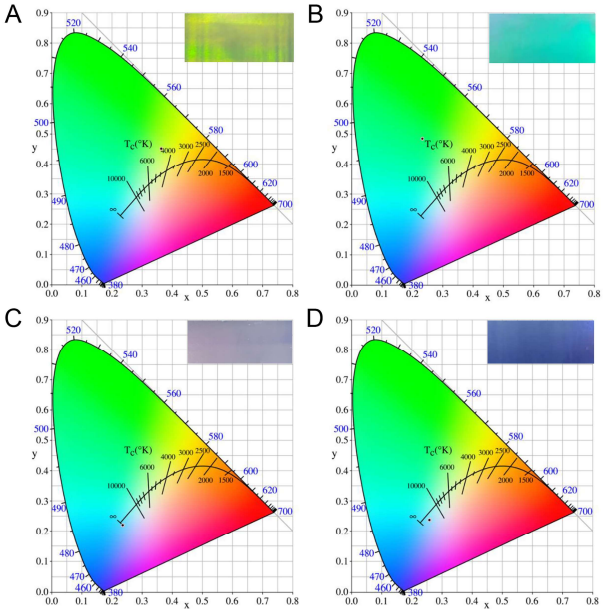

Figure S6. CIE (International Commission on Illumination) chromaticity diagram showing the (x, y) color coordinates of CPC, inset: Digital photograph of CPC: (A) CPC_{230}, (B) CPC_{250}, (C) CPC_{300}, (D) CPC_{320}.

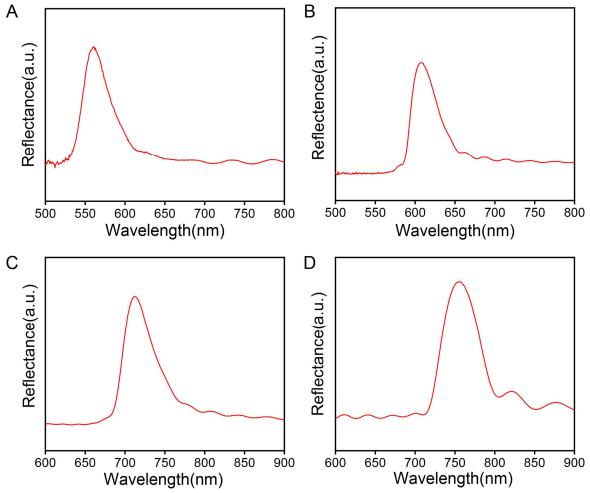

Figure S7. Reflectance spectra of fabricated colloidal photonic crystal: (A) CPC_{230}, (B) CPC_{250}, (C) CPC_{300}, (D) CPC_{320}.

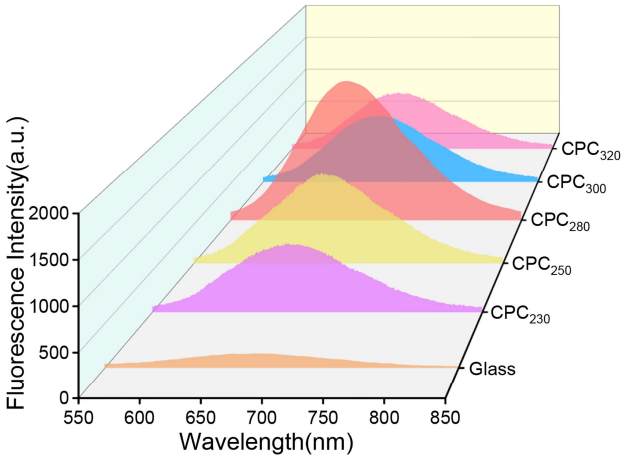

Figure S8. Fluorescence spectra of BSA-AuNCs on different PS-CPC films (glass, CPC_{230}, CPC_{250}, CPC_{280}, CPC_{300}, and CPC_{320}).

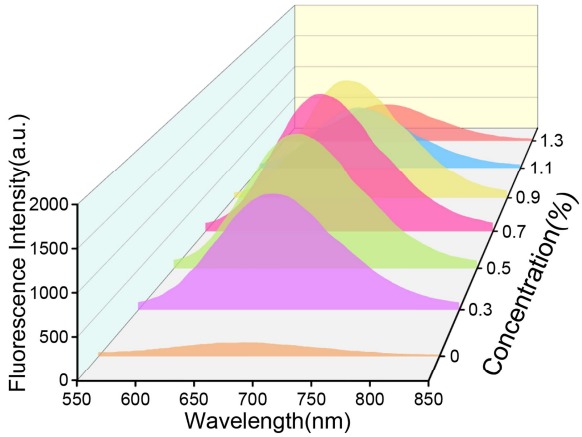

Figure S9. Fluorescence spectra of BSA-AuNCs based on the CPCs with different concentration of PS.

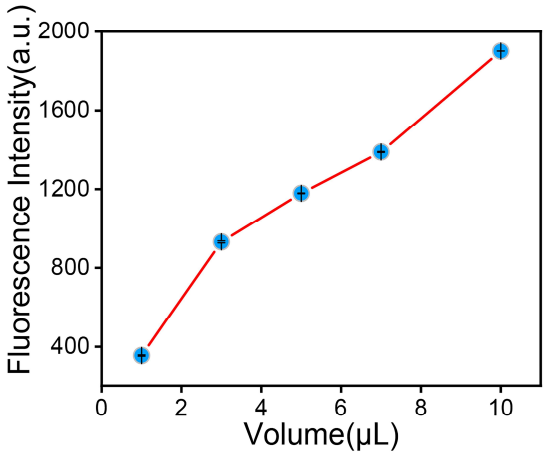

Figure S10. Fluorescence intensity of BSA-AuNCs-CPC with different BSA-AuNCs volumes.

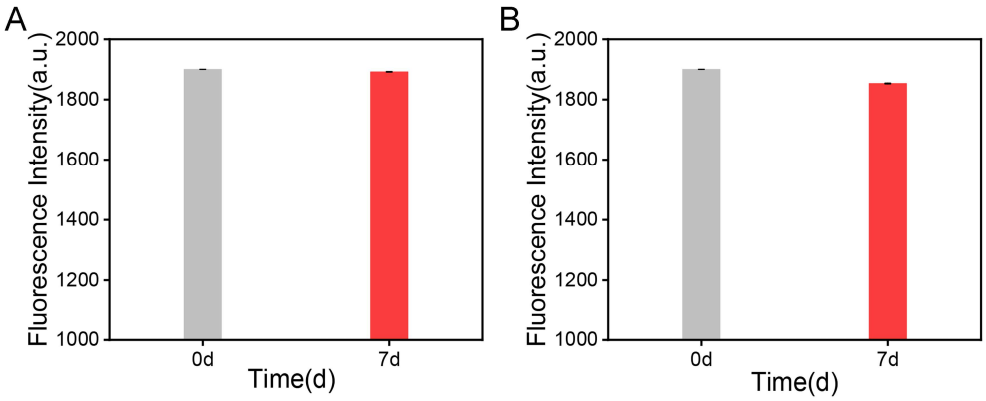

Figure S11. (A) Fluorescence intensity of BSA-AuNCs stored for 0 and 7 days. (B) Fluorescence intensity of BSA-AuNCs-CPC stored for 0 and 7 days.

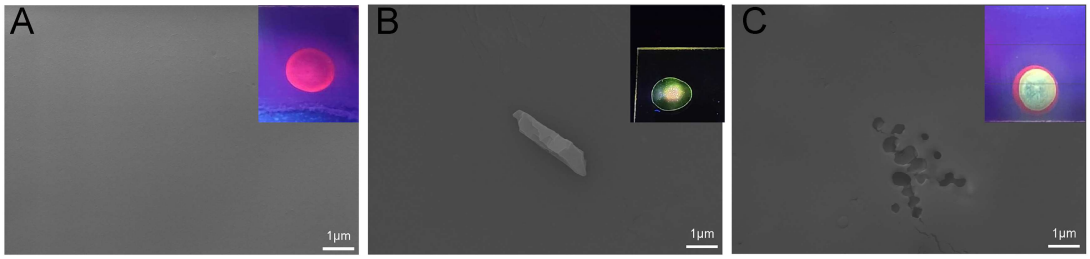

Figure S12. SEM images of (A) BSA-AuNCs-CPC, (B) OTC, (C) BSA-AuNCs-CPC + OTC. Inset: the corresponding fluorescent images under the irradiation of a 375 nm laser source.

Table S1 Comparison of fluorescence assay for determination of OTC.

Probe used in literature	Detection range(nM)	Detection limit(nM)	Ref.
LTN@AuNCs[1]	500-1.5×10^4	300	[4]
QDs@porous carbon[2]	10-10^5	3.23	[5]
SiO_2/Ag@FMIPs[3]	0-300	5.38	[6]
CuNCs@PEI[4]	500-3×10^5	32	[7]
NH_2-UIO-66(Zr)@MIP[5]	109-8.7×10^4	26.06	[8]
AuNP@MIPs-CdTe QDs[6]	100-3×10^3	5.22	[9]
NiNCs-Eu^{3+} [7]	100-5×10^4	21	[10]
CDs@LP[8]	0-2×10^4	3.2	[11]
BSA-AuNCs-CPCs	2-1×10^4	1.03	This work

LTN[1]: L-tryptophanonitrile; QDs@porous carbon[2]: Quantum dots combined with porous carbon; FMIPs[3]: molecularly imprinted polymers containing a sensitive fluorophore; PEI[4]: polyethyleneimine; NH_2-UIO-66(Zr)@MIP[5]: molecularly imprinted polymer-coated amino-functionalized zirconium (IV) metal–organic framework; AuNP@MIPs-CdTe QDs[6]; molecularly imprinted polymers (MIPs)-isolated AuNP-enhanced fluorescence; NiNCs-Eu^{3+} [7]: nickel nanoclusters (NiNCs)-europium complex; CDs@LP[8]: carbon dots-based luminophore.

Table S2 Comparison of photonic crystal enhanced fluorescence methods

detection object	enhancement fold	limit of detection	references
rhodamine B	150	-	[12]
Cu^{2+}	17	0.34 nM	[13]
Cr (VI)	100	0.2 ppb	[14]
acetylcholinesterase paraoxon	10	0.027 mU/mL, 0.025 ng/mL	[15]
adenosine	10	1.3 × 10^{-6} mol L^{-1}	[16]
nitrite	-	0.25 μmol/L	[17]
oxytetracycline	11.9	1.03nM	this work

3. References

1. K. Shen, L. Zhang, X. Chen, L. Liu, D. Zhang, Y. Han, J. Chen, J. Long, R. Luque, Y. Li and B. Chen, *Science*, 2018, **359**, 206-210.
2. M. M. Thomas, A. Babu, P. R. Chandran, S. T. S and S. Pillai, *Chem.-Asian J.*, 2023, **18**, e202201035.
3. D. Li, Z. Chen and X. Mei, *Adv. Colloid Interface Sci.*, 2017, **250**, 25-39.